December 1980 LRP 176/80

IDEAL MHD STABILITY OF OBLATE SPHEROMAKS AND β OPTIMIZATION

P. Gautier, R. Gruber, and F. Troyon

Ideal MHD Stability of Oblate Spheromaks and β Optimization

P. Gautier*, R. Gruber, and F. Troyon

Centre de Recherches en Physique des Plasmas

Association Euratom - Confédération Suisse

Ecole Polytechnique Fédérale de Lausanne

CH-1007 Lausanne / Switzerland

ABSTRACT

An oblate spheromak surrounded by a conducting shell can stably confine a plasma with non-vanishing pressure. Using the ERATO code we find that whenever $q_{axis} \gtrsim 1$ an internal kink develops, while for $q_{axis} < 1$ the Mercier criterion limits the β value. This leads to a β limit which increases with the aspect ratio. For an aspect ratio of 2.4, equilibria with $\beta \gtrsim 40\%$ have been found which are stable to both low-n and high-n modes. Without a shell these equilibria are unstable; the fastest growing mode being a n = 1 tilting motion. A shell at a distance of the order of 0.2 - 0.4 the minor plasma radius stabilizes the low-n modes.

* presently at Max-Planck Institut für Plasmaphysik (IPP), Garching, Germany

I. INTRODUCTION

First introduced to designate a very specific configuration, characterized by a spherical plasma in which flows a force-free current and with no externally-applied toroidal field {1, 2, and 3}, the word "Spheromak" is now used to describe any toroidal axisymmetric configuration in which the toroidal field vanishes at the plasma surface { 4 }. It can be viewed as limit of a Tokamak when either the toroidal current increases indefinitely or the external toroidal field vanishes, while keeping the poloidal beta β_p constant. The potential advantages of this configuration have already been spelled out in Bussac et al. {4} which also contains additional references. But there remain many unsolved problems. One of them is to understand the difference in the stability properties between a Tokamak and a Spheromak, to find out if there is a β limit, how high it is and how it depends on the geometrical and physical parameters.

M. N. Rosenbluth and M. N. Bussac have laid the groundwork by studying the MHD stability of the genuine spheromak, identifying the relevant parameters { 5 }. The genuine spheromak is defined by the flux function $\psi(r,z)$:

$$\psi(r,z) = \frac{r^2}{\sqrt{r^2+z^2}} \; j_1\left(\gamma \frac{\sqrt{r^2+z^2}}{a}\right), \tag{1}$$

where r,z,θ are cylindrical coordinates centered on the main axis of the torus, $\gamma \sim 4.493$ is the first zero of the spherical Bessel function $j_1(x)$ and a is the radius of the spherical plasma boundary on which $\psi = 0$.

The current density $\underline{J}$ is obtained from the Grad-Shafranov equation

$$\underline{J} = \sqrt{\frac{\gamma}{a}}\ \underline{B}. \tag{2}$$

It is clearly force-free. The toroidal magnetic field is given by

$$B_T \equiv \frac{T(\psi)}{r} = \sqrt{\frac{\gamma}{a}}\,\frac{\psi}{r}\ . \tag{3}$$

Keeping the same expression (2) for the current density, more general equilibria can be obtained having still the same spherical topology but different shapes. Such a solution, which has been studied in some detail by the previous authors [5], is

$$\psi(r,z) = \frac{r^2}{\sqrt{r^2+z^2}}\left\{j_1\left(\frac{\gamma}{a}\sqrt{r^2+z^2}\right) + \varepsilon\,\frac{4z^2-r^2}{r^2+z^2}\ j_3\left(\frac{\gamma}{a}\sqrt{r^2+z^2}\right)\right\}, \tag{4}$$

where ε is a free parameter. The plasma surface is given by the condition $\psi(r_s,z_s) = 0$, namely

$$j_1\left(\frac{\gamma}{a}\sqrt{r_s^2+z_s^2}\right) + \varepsilon\frac{4z_s^2 - r_s^2}{r_s^2 + z_s^2}\, j_3\left(\frac{\gamma}{a}\sqrt{r_s^2+z_s^2}\right) = 0 . \qquad (5)$$

For $\varepsilon = 0$ the shape is again a sphere. For $\varepsilon > 0$ the plasma is elongated (prolemak) and for $\varepsilon < 0$ it is flattened along the axis $r = 0$ (oblimak).

By expanding around $\varepsilon = 0$, Rosenbluth and Bussac have shown a prolemak is unstable to global internal tilting, while an oblimak is stable to such displacement. They have also shown that the oblimak is unstable to free boundary modes for all $n > 1$, but a shell at a distance of the order of .15a stabilizes low-n modes. High-n modes are always unstable but non-ideal MHD effects or a modification of the current profile at the plasma surface are thought to take care of these modes, so that with a shell an oblimak should be stable.

But this is still a $\beta = 0$ plasma. The maximum pressure which can be stably confined by this configuration is limited by the Mercier criterion. The maximum value of β quoted in {5} is less than $1\,^{o}/oo$. The reason for such a low value is the low shear of the configuration. Excluding the plasma current from a central hole, creating a fat torus with $B_T = q = 0$ at the surface, increases shear and thus the β allowed by Mercier. Numerical calculations {4} and analytic estimates {5} have confirmed that the maximum β increases with the size of the hole. In the limit of a large aspect ratio and a circular cross-section a value of $\beta_{max} \sim 15\%$ is quoted. The stability of low-n modes has only been studied for the pressureless case, without a hole, using the Taylor

criterion.

In this paper we pursue this same problem of β limitation due to the onset of ideal MHD instabilities. The objective is to study as completely as possible, using an ideal MHD stability code for low-n modes {6}, and the ballooning and Mercier criterion for localized modes, a wider class of equilibria which includes as special cases the geometry and profiles treated analytically in {5}, so that useful comparisons and verifications can be made. The picture which emerges from these calculations is simple and should have a wide range of applicability.

The results can be summarized as follows. The stability of internal modes of an oblimak is controlled mainly by shear and by the safety factor on axis q_o. For $q_o \lesssim 1$, the Mercier criterion is a necessary and sufficient condition for stability. The higher the shear, the higher the β. The higher q_o, the higher the shear. But for $q_o \gtrsim 1$, an internal n = 1 unstable kink appears. This leads to a unique prescription for β optimization, namely to increase shear as much as possible while keeping q_o around 1. For a given q_o, the shear becomes more uniform as the size of the central hole increases and this leads to higher stable values of β. These results are obtained with a shell right on the plasma surface. Without a shell the plasma is always unstable. The n = 1 tilting mode is the most dangerous of the low-n modes with an extremely large growthrate. Higher-n modes are much less unstable. A shell at a distance of the order of 0.2 to 0.4 the minor

plasma radius stabilizes the low-n modes. High-n modes must still be unstable with such a shell, but it is reasonable to ascribe to the current jump at the plasma surface the residual instabilities. An adjustment of the current profile at the surface should take care of all these modes except n = 0 and n = 1, and maybe n = 2. Free boundary stability appears to be the only real difficulty for the spheromak configuration, within the framework of ideal MHD, and should be studied by introducing more general shapes.

The plan of the paper is the following: We first define the class of equilibria, introducing four free parameters. We then study in detail the stability of internal modes of a typical oblimak with a small hole, keeping the shape fixed and varying the force-free current profile as well as the pressure profile. This leads to the β optimization procedure which is used to study the dependence of β_{max} as a function of the size of the hole. The transition oblimak-prolemak is not examined. We then study the stability of free boundary modes, without any shell, starting first with the same typical oblimak and then varying the size of the hole. A shell is introduced and its effect on the low-n modes is briefly studied. It ends with a discussion of some interesting convergence properties of the ERATO code, the ideal MHD stability code used in all these calculations, which seem to be specific to spheromak configurations.

II. THE EQUILIBRIUM CONFIGURATION

The equilibrium is specified by giving the 2 source terms $dp/d\psi$ and $T\frac{dT}{d\psi}$ in the Grad-Shafranov equation,

$$\Delta^*\psi = -r^2\frac{dp}{d\psi} - T\frac{dT}{d\psi}, \tag{6}$$

and by the shape of the plasma boundary. The current density $\underline{J}$ can be written as

$$\underline{J} = r\frac{dp}{d\psi}\underline{\hat{e}}_\phi + \frac{dT}{d\psi}\underline{B}, \tag{7}$$

where $\underline{\hat{e}}_\phi$ is in the toroidal direction. We see that T contributes only to the force-free current.

For the current flux T, we choose

$$T^2 = C_1\psi^2(1 + \frac{2}{3}\alpha\psi), \tag{8}$$

where α is a new free parameter which allows a certain degree of control over the current and q profiles. The flux ψ is chosen to vanish on the boundary and be negative inside.

As for the pressure profile, we should like to determine it implicitly by the constraint that the Mercier criterion be marginal everywhere. This is inconvenient for the equilibrium code which has to be run with a high resolution because of the requirements of the stability code ERATO. We have instead chosen an analytic form

$$\frac{dp}{d\psi} = C_1 C_2 (\psi_o - \psi), \tag{9}$$

where ψ_o is the value of ψ on the magnetic axis. This dependence is the simplest one which can satisfy the Mercier criterion on the magnetic axis, while having the same qualitative behavior as the optimal pressure gradient given by the Mercier criterion. This means the maximum β which can be stably confined is underestimated, but on the other hand, the expression (9) leads to an unphysical current discontinuity at the surface which should be smoothed out, and this will decrease β.

As plasma boundary, we use one of the magnetic surfaces of the spheromak equilibrium given in Eq. (4), namely

$$\frac{\delta r_s^2}{aR} \left\{ j_1\left(\frac{\delta}{a}R\right) + \epsilon \frac{4z_s^2 - r_s^2}{R^2} j_3\left(\frac{\delta}{a}R\right) \right\} = \delta, \tag{10}$$

where $R \equiv (r_s^2 + z_s^2)^{\frac{1}{2}}$ and δ is a free parameter which measures the size of the central hole, or, equivalently, the aspect ratio. In this way we can study some features of the spheromak without a hole by extrapolating the results with $\delta \neq 0$ to $\delta = 0$. The original spheromak is recovered when $\delta = 0$, $\alpha = C_2 = 0$.

In the general case, we fix C_1 by the condition that the total toroidal current I_T,

$$I_T = - \iint dr dz \left\{ r \frac{dp}{d\psi} + \frac{T}{r} \frac{dT}{d\psi} \right\}, \tag{11}$$

be constant and equal to its value when $\delta = \alpha = C_2 = 0$, namely $I_T = 2$. There remain only 2 free parameters to specify the profile, α and C_2 or, equivalently, q_o and β, where the volume averaged β is defined as

$$\beta = \frac{\iint p \; r \; dr \; dz}{\iint \frac{B^2}{2} \; r \; dr \; dz} . \tag{12}$$

When $\alpha = C_2 = 0$, the current profile is peaked; increasing α flattens the current on the magnetic axis and eventually a hollow current profile develops. This behavior is mirrored in the q profile which peaks as α increases. Keeping α constant, increasing C_2 increases β with no effect on the q profile and little effect on the current until the fraction associated with the pressure gradient becomes a sizeable fraction of the force-free current. Figures 1 and 2 illustrate the dependence on α for a specific configuration: an oblimak with $\varepsilon = -.3$, $\delta = .2$, which will be referred to as "standard case".

Note that the quantity ε determines the elongation, but that it is not equal to it, while δ measures the size of the hole or, equivalently, the aspect ratio. The shape of the plasma cross-section varies with δ (Fig. 3); the maximum value of δ is 1.18.

III. STABILITY OF INTERNAL MODES OF THE STANDARD CASE

We first assume there is a shell tight on the plasma so that we only look at internal modes.

The high-n stability is determined by the ballooning criterion. On the magnetic axis it coincides with the Mercier criterion, but everywhere else it should be more stringent. The ballooning criterion becomes difficult to implement whenever the shear is low or the ballooning weak because the range of integration becomes so large that inaccuracies in the equilibrium quantities, as well as in the integration, become dominant. Near the magnetic axis, for example, it is not possible to verify directly the agreement between the Mercier and ballooning criteria with numerical equilibria. In all the spheromak calculations we have made, the ballooning limit has been found to be less stringent than Mercier's limit, although the range of integration is the same as that used in our calculations of β limits in Tokamaks. This means the balloon-

ing limit is very close or maybe even coincides with Mercier's limit throughout the plasma. This is consistent with the results obtained in Tokamaks which have $\beta_p < 1$, and with the fact that, away from the axis where a difference is expected, the poloidal field dominates the toroidal field ($q << 1$), thus removing the main factor responsible for the ballooning effects in Tokamaks. The impossibility of obtaining a ballooning unstable region as wide as the Mercier unstable region, wherever $q' < 0$, has also been observed by J. Greene and M. Chance {8}. It is probably an indication of very localized and very weakly growing modes.

The Mercier criterion can be written as {7}

$$\frac{1}{4}\left(\frac{dq}{d\psi}\right)^2 + M_1(\psi)\frac{dp}{d\psi} + M_2(\psi)\left(\frac{dp}{d\psi}\right)^2 \geq 0, \tag{13}$$

where

$$M_1(\psi) \equiv T^2 G_{43} \frac{dG_{01}}{d\psi} + \frac{q}{T}\frac{dG_{01}}{d\psi} - T\frac{dq}{d\psi}G_{23}, \tag{14}$$

$$M_2(\psi) \equiv T^2\left[G_{23}^2 - G_{03}G_{43}\right] - G_{21}G_{03},$$

$$G_{\alpha\beta}(\psi) \equiv \oint \frac{d\ell}{r^\alpha B_p^\beta}, \tag{15}$$

and B_p designates the poloidal field. At low β, the quadratic term in $dp/d\psi$ is negligible and $M_1(\psi)$ only depends on the force-free current distribution TT'. For $\alpha = 0$, $M_1(\psi) > 0$ everywhere and the condition (13) gives the condition

$$\frac{dp}{d\psi} \geq -\frac{1}{4}\left(\frac{dq}{d\psi}\right)^2 / M_1(\psi). \tag{16}$$

Near the magnetic axis, the right-hand side of Eq. (16) varies linearly as $\psi - \psi_o$. As long as $q_o < 1$, this condition limits $dp/d\psi$ everywhere, and the integration of the right-hand side gives a maximum pressure which can be stably confined. Figure 4 shows the limit given by Eq. (16) for a typical case. Since $dp/d\psi$ is largest at the edge, the pressure profile must be very flat. Our linear parametric form for p' (9) has the same general behavior around the axis as the optimal choice. This is the main reason for this choice.

With these profiles, the complete Mercier criterion (13) leads to an upper limit on C_2 which is a function of α. This is shown for the standard case in Fig. 5. The limiting C_2 is an increasing function of α. As β increases with both α and C_2 the highest stable values are obtained in the upper right-hand corner of the Mercier

stable region, which means the largest value of α. But as α increases, becomes greater than 1. Increasing α much beyond this point leads, for large δ, to numerical problems with the stability code because of the appearance of a current reversal. But for the standard case, this is not the limiting factor on α. It is the low-n stability which sets a limit on α.

The low-n stability is tested with ERATO. We first look for unstable modes in the Mercier stable regime, and more particularly in the large α region. We find that n = 1 becomes unstable whenever q_o increases much above 1. The mode is definitely an internal kink, as can be seen in Fig. 6. It is m = 1 and the maximum shear displacement occurs on the q = 1 surface. The motion is internal and the growthrate small. Figure 7 shows the square of the growthrate as a function of α, or q_o, for various values of C_2. The normalizing growthrate ω_A is given by

$$\omega_A = B_o \Big/ \sqrt{\rho_o R_m^2} \quad , \tag{17}$$

where B_o, ρ_o and R_m are, respectively, the magnetic field, density and radius at the magnetic axis. The marginal points are definitely above $q_o = 1$. The influence of the pressure is stabilizing and only seen in the growthrate, which means the mode is current driven. The

difference between the marginal point and $q_o = 1$ appears meaningful and not due to lack of resolution, as shown in section 7. In the same region, below the Mercier limit, no $n < 5$ unstable mode has been found with the highest resolution used. Since we do not expect high-n unstable modes in the ballooning stable region we conclude that the only instability which limits α is the internal kink $n = 1$.

In all Tokamak configurations we have studied, whenever the Mercier criterion is violated on one of the singular surfaces corresponding to a given n (nq integer), there are rather global unstable modes with the same n. This means that, for Tokamaks, the violation of the Mercier criterion is a warning of the existence of a dangerous instability. We expected the same behavior in the spheromak regime. On the other hand, the difficulties encountered with the ballooning criterion suggested that the Mercier unstable modes are very weakly growing. To clarify this problem, we search for low-n unstable modes in the Mercier unstable region pictured in Fig. 5.

The Mercier unstable regions for each $n \leq 5$ are shown in Fig. 8. They are obtained by verifying the Mercier criterion on each singular surface $q = m/n$, where m is an integer which also happens to be the dominant poloidal mode number of the most dangerous localized modes.

For n = 1, there are no singular surfaces within the plasma as long as $q_o < 1$ and Mercier is satisfied on the q = 1 surface when $q_o > 1$. Up to $C_2 = 0.01$ (largest value tested), no n = 1 unstable mode has indeed been found in the range $q_o \tilde{<} 1$, while for larger q_o the unstable mode is an internal kink as shown above.

For n > 1, we look first for the most unstable mode along the axis $\alpha = 0$, varying $C_2(\beta)$. The results for n = 2 are shown in Figs. 9 - 11. Figure 9 shows a map of the poloidal component of the displacement vector of the most unstable mode for decreasing values of C_2: .010, .008, and .006 respectively. As C_2, respectively β, decreases, so does the growthrate, and the mode becomes more and more localized around the only singular surface within the plasma at q = 0.5. At the marginal point it will turn into the marginal continuum mode resonant on the q = 0.5 surface ($\Delta = 0$). This mode has all the expected features of a Mercier mode and never seen with a Tokamak profile ($q' > 0$)! The potential energy associated with a displacement $\underline{\xi}(\psi,\chi)e^{in\phi}$ can be written as

$$\delta W = \int_o^1 ds \oint d\ell \; \delta W_n \equiv \int_o^1 ds < \delta W_n >, \tag{18}$$

where s is a radial variable related to the flux ψ through $s = \sqrt{(\psi_o - \psi)/\psi_o}$. $<\delta W_n>$ is the flux averaged potential energy density. Figure 10 shows $<\delta W_2>$ for the same 3 modes. The normalization has been chosen such that $\int_o^1 ds|<\delta W_n>|$ be the same. There is a large cancellation between two positive contributions (stabilizing) and a deep negative contribution from the singular surface. As β decreases, the cancellation becomes more and more complete and the width of the negative hole becomes narrower. Figure 11 shows the full width Δ of the region where $<\delta W_2>$ is negative as a function of β. The extrapolated value of β at which $\Delta = 0$, β_c, corresponds well with the Mercier limit. The localization and the cancellation cause numerical difficulties and explain our incapacity to follow the mode down to the Mercier limit. But it also implies that, for n = 2, the Mercier limit is the true limit.

Since $q < 0.6$, there is also only one singular surface, $q = 1/3$, for n = 3. It is located on the outside of the plasma in a region of high shear and the growthrate is much smaller than for n = 2. For n = 4, there are 2 singular surfaces, $q = 1/2$ and $q = 1/4$, the second one being very near the plasma surface and Mercier stable up to very high values of β. The most unstable mode is localized around $q = 1/2$, with a growthrate close to the n = 2 mode. In all these cases the potential energy has the same behavior as for n = 2, which implies a stability limit given precisely by the Mercier criterion. The width of the unstable region around $q = 0.5$ is also shown in Fig. 11. The extrapolated limit on β is consistent with the n = 2 limit. The growthrate is related to the localization

of the most unstable mode. Modes localized on singular surfaces which lie in the outer region or close to the axis are slower growing. The correlation is particularly clear for n even (tested up to n = 6), in which case the most unstable mode is localized on q = 1/2 and the growthrate seems independent of n. How high n has to be in order to have a true ballooning mode extending across many singular surfaces is still an open question.

All these modes have been obtained at high values of C_2, corresponding to high values of β. Already for $C_2 = .006$, corresponding to $\beta = 8.5\%$, the modes are so localized that we have great numerical difficulties to obtain them and the growthrates are of the order of $10^{-2} - 10^{-3}\ \omega_A$. Non-ideal MHD corrections or non-linear corrections will already strongly affect such modes, probably stabilizing them.

Varying α does not change the basic results and the conclusion of this study is the confirmation that stability of low-n modes is less restrictive than the overall Mercier criterion, and that, in the Mercier unstable range, the modes are very localized and the growthrates very small up to substantial values of β (a few percents).

IV. β OPTIMIZATION

We have established for our standard oblimak that the requirement of stability of internal modes imposes both a limit on C_2 given by Mercier and an α given by the appearance of the internal kink. The highest stable value of β is obtained when C_2 and α assume their limiting values, which for this case gives a $\beta_{max} = 12$ %.

In order to study the dependence of β_{max} on the size of the hole (aspect ratio), we should have to repeat the same calculation for various values of δ. Because of the prohibitive amount of computing time needed to obtain precisely the internal kink limit, we have chosen a more conservative approach by assuming that the internal kink limit is $q_o = 1$ and calculating only the Mercier limit.

The results of this optimization is shown in Fig. 12. The dispersion of the points reflects the accuracy of the optimization. The optimization requires computing a large number of numerical equilibria and it was stopped at q_o reasonably close to 1 with the Mercier criterion tested on 40 magnetic surfaces. The largest value of δ considered corresponds to an aspect ratio of 2.34. The increase of β_{max} with δ is at first puzzling, but looking at the q profile we see that with larger δ the shear becomes better distributed across the plasma, which leads to a higher stable pressure gradient. It is not an artifact of the functional dependence of the pressure gradient

(Eq.(9)), since the integration of the Mercier limit $(\frac{dp}{d\psi})_{max}$ given in Eq. (16) leads to the same dependence. The essential point is the existence of MHD stable very high β equilibria with already a small aspect ratio. The extrapolated value of β_{max} at $\delta = 0$ is of the order of 1.5%, an improvement of more than an order of magnitude over the original spheromak profile.

V. FREE BOUNDARY STABILITY

Without a conducting shell, all the spheromaks studied here have been found unstable to free boundary modes. The most unstable mode is a n = 1 tilting, at least for the value of ε studied here. This result confirms and extends the analytic result of Bussac and Rosenbluth [5]. Figure 13 shows the growthrate of this tilting mode as a function of the size of the hole, δ, always for the same oblimak with $\varepsilon = -.3$, with no pressure ($\beta = 0$) and no current modification ($\alpha = 0$). It is very fast, of the order of one Alfvén transit time across the plasma radius, and insensitive to the size of the central hole. Such a mode is represented in Fig. 14. It is a tilting motion, although it is more complicated than the rigid tilting used as trial displacement in the analytical calculations mentioned above. Increasing the pressure increases the growthrate slightly. No profile modification can affect such a fast growing mode.

There is a n = 2 unstable mode. Its growthrate is shown in Fig. 13 for the same set of equilibria. It is slower growing than the n = 1 mode. A typical poloidal plot of such a mode is represented in Fig. 15. It looks also like a tilting, but since it is n = 2, it tilts in opposite directions at 180^{o} around the torus, filling the central hole.

A typical radial flux averaged potential energy distribution $\langle \delta W \rangle$, as defined in Eq. (18), is shown in Fig. 16. For n = 1, all the plasma, except for the immediate vicinity of the surface, gives a destabilizing contribution, while, for n = 2, it is only the region between $q \overset{\sim}{\sim} 1/2$ and the surface which is unstable. No n = 3 unstable mode has been found in this case (δ = 0.2) with the highest resolution. But when there is a pressure (but still in the Mercier stable region) all n become unstable, although the growthrate rapidly decreases with n. The average potential energy $\langle \delta W \rangle$ has the same general behavior shown in Fig. 16 for n = 2, the unstable region being mainly between the q = 1/n surface and the plasma surface. This suggests that by shaping the current profile at the edge so that the current, as well as its slope, vanishes on the plasma surface, all high-n free-boundary modes will become stable. There should only remain the n = 1 tilting and maybe the n = 2.

The absence of an unstable n = 3 mode in the pressureless case is very surprising since we know {5} that for $\delta = 0$ all n are unstable. It may be that the highest resolution we have used is not yet sufficient to bring it out, in which case the growthrate would be very small and our conclusions unaffected. The other possibility is a stabilizing effect of the shear at the edge due to the hole.

In all these cases there is an unstable n = 0 mode. All these calculations have been made with no wire on the axis of the torus.

VI. SHELL STABILIZATION

Among the results obtained by Bussac and Rosenbluth figure a study of the influence of a conducting shell on free boundary modes of a spheromak, predicting that a shell at a short distance from the plasma would stabilize the low-n modes.

We have introduced a shell surrounding all the plasma which, for technical reasons, goes through the hole of the plasma. When the hole is small the shell covers the hole, but inside there is still a wire on the axis. This wire has no influence on $n \geq 1$ modes as we have verified by recalculating the case of an infinite vacuum without a wire on axis. The same test on the $n = 0$ instability has shown very strong stabilization so that we do not consider this case.

The results for our standard shape, $\varepsilon = -.3$ and $\delta = .2$, and with the highest β stable ($\beta \tilde{\sim} 12\%$) to all internal modes, are shown in Fig. 17. The square of the growthrate of the most unstable modes is plotted versus a parameter R_{ext}, which measures the distance between the shell and the plasma surface. The shell is given by the equation

$$\rho^{(\theta)}_{shell} = \rho^{(\theta)}_{plasma} + (R_{ext} - 1)\, a, \tag{19}$$

where $\rho(\theta)$ is the distance from the magnetic axis, θ the angle around the magnetic axis, and a half the plasma width in the equatorial plane. If the shell, as described by Eq. (19), intersects the axis of the torus for an angle θ_{max}, the section $\theta_{max} < \theta < 2\pi - \theta_{max}$ is replaced by a wire on the axis. We find that stability is achieved, for all the low-n modes studied, when the shell is at a distance of the order of .35 a. The same result holds for any δ, the maximum distance between the shell and the plasma varying between .2 and .4 a, the distance being larger for a smaller hole.

VII. CONVERGENCE PROPERTIES OF E R A T O

ERATO is not a true finite element code. The variation of the Lagrangian is done on an enlarged functional space. This enlarged functional space is expected to lead to a lower energy state, and thus to a destabilizing effect. The integration error is of the same order in h^2 and could either reinforce or counterbalance the destabilization. But in all the numerous Tokamak calculations done with ERATO {9}, it has been observed that the net effect is destabilizing, and this has turned out to be a strong practical advantage in studying stability limits. At low resolution, there is an unstable mode and, to determine if there is stability, the growthrate and mode structure are followed as resolution is increased. In this way an upper limit to the growthrate is always obtained and since we always obtain the mode, we can usually identify the transition to a stable continuum mode.

With spheromaks we have observed the opposite behavior. At low resolution, we usually do not find an unstable mode. The first mode is the slow marginal continuum mode which we know and it is indeed very close to $\omega^2 = 0$. If the plasma is unstable, as resolution is increased,

the first mode suddently changes in structure and the convergence plot shows a sharp break. A typical case is shown in Fig. 18. This is a definite drawback which ERATO shares with PEST and any other potential codes which are based on a variational formulation of the energy principle. In any situation, stability is never certain since more resolution may bring out a new unstable mode, and, even worse, the uncertainty cannot be quantified. These difficulties translate into high costs since many runs have to be made with the highest resolution.

There is a limit on the largest value of n which can be handled with the code. It is function of the resolution. For high n, we know that any unstable mode has a ballooning poloidal dependence

$$\underline{\xi}(\psi,\chi) = \tilde{\underline{\xi}}(\psi,\chi)e^{inq\chi}, \tag{20}$$

where $\tilde{\underline{\xi}}$ is slowly varying in χ. The poloidal angle χ is related to the arc length ℓ along a meridian cross-section of the magnetic surface ψ by

$$\chi \equiv \int_o^{\ell} \frac{T d\ell}{qr^2 B_p} . \tag{21}$$

As n increases, the fast phase variation in the χ direction becomes impossible to reproduce. The relevant parameter is nq, which gives the number of periods of the fast oscillation, and it is practically

limited to $nq \lesssim 5\text{-}10$. Because of the low q values typical of spheromaks, it should be possible to study modes up to $n \sim 5\text{-}15$, depending on q_o, but the radial resolution needed to represent correctly the mode near each singular surface becomes the limiting factor.

VIII. ACKNOWLEDGMENTS

This work has been done in many stages and we have benefited from many discussions and unpublished material from M.N. Bussac and M.N. Rosenbluth, especially in the phase where we were feeling our way and relied heavily on their analytic results to provide clues and checks. The calculations have been done in Lausanne and Garching (IPP) with full cooperation of the computing staffs. We thank W. Schneider for his help in implementing the equilibrium code in Garching.

This work has been supported by the Swiss National Science Foundation, the Ecole Polytechnique Fédérale de Lausanne, and by Euratom.

REFERENCES

{1} Lüst, R., Schlüter, A., Z. Astrophys. 34 (1954) 263.

{2} Chandrasekhar, S., in Proc. of the National Academy of Sciences, 42 (1956) 1.

{3} Alfvén, H., in Proc. 2nd Int. Conf. on Peaceful Uses of Atomic Energy, 31 (1958) 3.

{4} Bussac, M.N., Furth, H.P., Okabayashi, M., Rosenbluth, M.N., and Todd, A.M.M., in Plasma Physics and Controlled Nuclear Fusion Research (Proc. 7th Int. Conf. Innsbruck, 1978) Nuclear Fusion Supplement, IAEA, Vienna (1979), Vol. III, 249.

{5} Rosenbluth, M.N., Bussac, M.N., Nuclear Fusion 19 (1979) 489.

{6} Gruber, R., Troyon, F., Berger, D., Bernard, L.C., Rousset, S., Schreiber, R., Kerner, W., Schneider, W., Roberts, K.V. to be published in Computer Physics Communications (1981).

{7} Mercier, C., in Lectures in Plasma Physics, The Magnetohydrodynamic Approach to the Problem of Plasma Confinement, Commission of the European Communities, Luxembourg (1974) 140-146.

../..

References (cont'd)

{8} Greene, J., Chance, M., Sherwood Theory Meeting, Tucson, (April, 1980).

{9} Tsunematsu, T., Takeda, T., Matsuura, T., Kurita, G., Azumi, M., Computer Physics Communications, 19 (1980) 179.

FIGURE CAPTIONS

Fig. 1 : The toroidal current profile across the mid-plane of an oblimak $\epsilon = -.3$, $\delta = .2$, as a function of α.

Fig. 2 : The evolution of the q profile as a function of α for the same values of the parameters as in Fig. 1.

Fig. 3 : The shape of the plasma surface of the oblimak family $\epsilon = -.3$ as a function of δ (shown as a label). The aspect ratio is infinite for $\delta = 1.18$.

Fig. 4 : The limiting pressure gradient $dp/d\psi$ which makes the Mercier criterion marginal everywhere, Eq. (16), $s^2 = (\psi_o - \psi)/\psi_o$.

Fig. 5 : The Mercier stability diagram. The thick solid line separates the stable range (below) from the unstable region (above). In the unstable region, the lines labeled with a value of $s \equiv \sqrt{(\psi_o - \psi)/\psi_o}$ represent the stability limit given by the Mercier criterion on that particular surface. The lines β = constant are also shown.

Fig. 6 : Maps of the poloidal component of the eigenvector of an unstable mode in 2 meridian planes separated by 90^o, for $\alpha = 2.5$, $C_2 = .004$.

../..

Figure Captions (cont'd)

Fig. 7 : The growthrate of the internal kink as a function of C_2 and $q_o(\alpha)$.

Fig. 8 : The Mercier stability regions for n = 1, 2, 3, 4 and 5. For a given α and n, the stable region lies below the curve labeled with n. The discontinuity in the n = 3 curve is due to the appearance of an additional Mercier unstable singular surface deeper in the plasma as α increases.

Fig. 9 : Maps of the poloidal displacement in a meridian plane of the n = 2 most unstable internal mode for C_2 = .01, .008 and .006.

Fig. 10: The radial distribution of the potential energy density for C_2 = .01 (β = 14.9%), .008 (β = 11.8%) and .006 (β = 8.8%).

Fig. 11: The width of the unstable region Δ as a function of $\beta(C_2)$ for n = 2 and n = 4.

Fig. 12: The optimized β as a function of the size of the hole δ, for ε = -.3.

../..

Figure Captions (cont'd)

Fig. 13: The growthrate of the most unstable free-boundary modes $n = 1$ and $n = 2$, versus δ, for $\alpha = 0$, $C_2 = 0$ (pressureless spheromak) and $C_2 = .004/\beta = 5.6\%$). There is no shell around the plasma, nor any wire on the axis.

Fig. 14: Map of the poloidal displacement in a meridian plane of the $n = 1$ tilting mode for $\alpha = C_2 = 0$.

Fig. 15: Map of the poloidal component of the $n = 2$ free-boundary unstable mode for the same parameters as in Fig. 14.

Fig. 16: Radial distribution of the potential energy density $\langle \delta W \rangle$ for the same $n = 1$ and $n = 2$ modes, shown in Figs 14 and 15.

Fig. 17: Shell stabilization of free-boundary modes for $\alpha = 1.9$, $C_2 = .006$ ($\beta \sim 12\%$) close to the optimized β value for this geometry). There is a wire on the axis of the torus.

Fig. 18: Convergence plot for an internal kink mode with $\alpha = 1$, $C_2 = .002$. The square of the growthrate is plotted versus $1/N^2$. The mesh is made of N radial and 2N azimuthal intervals.

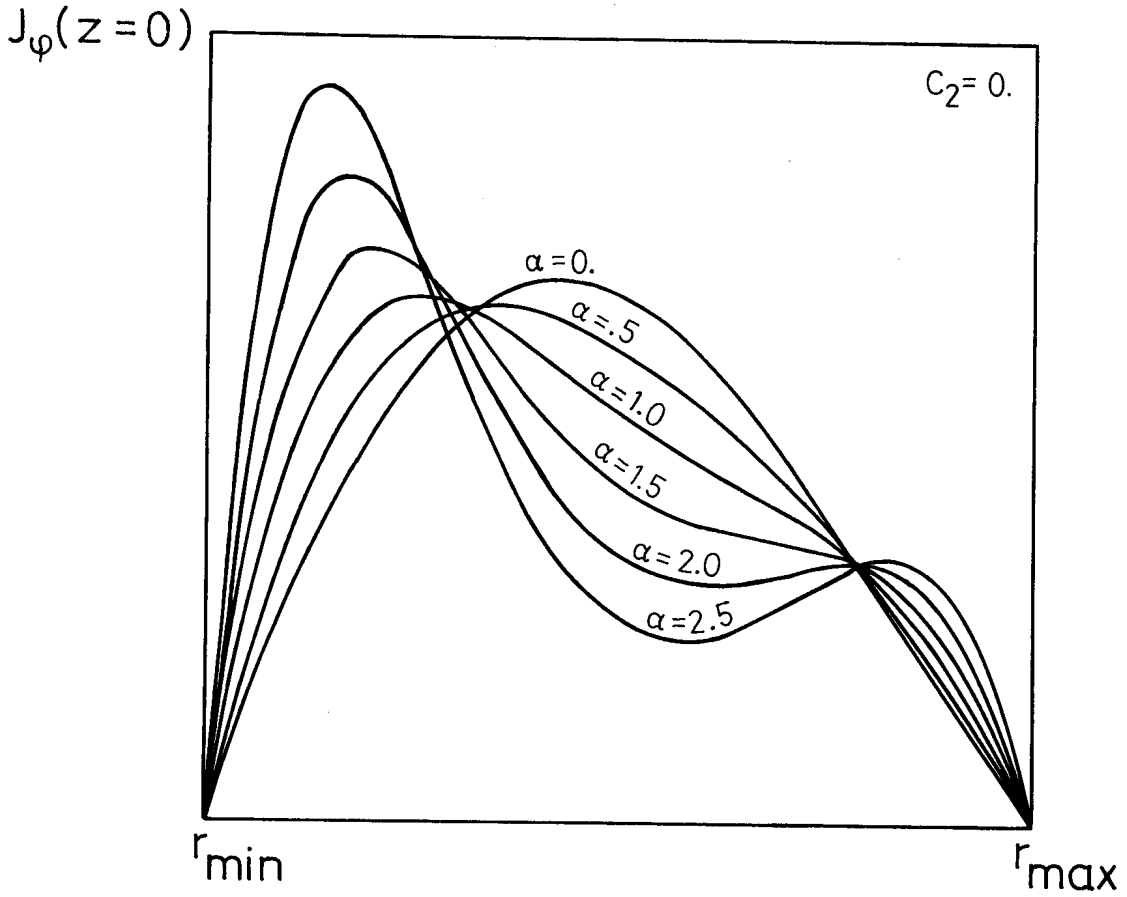
$J_\varphi(z=0)$
$C_2 = 0.$
$\alpha = 0.$
$\alpha = .5$
$\alpha = 1.0$
$\alpha = 1.5$
$\alpha = 2.0$
$\alpha = 2.5$
r_{min}
r_{max}

FIG. 1

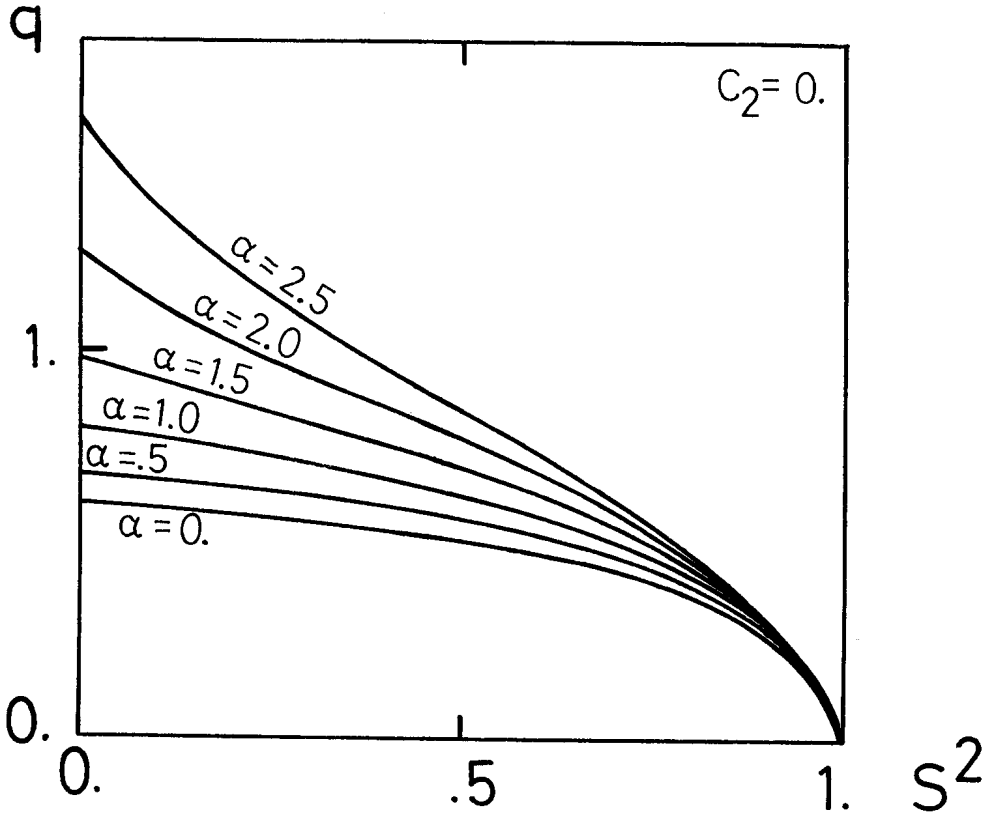
q
$C_2 = 0.$
$\alpha = 2.5$
$\alpha = 2.0$
$\alpha = 1.5$
$\alpha = 1.0$
$\alpha = .5$
$\alpha = 0.$
1.
0.
0.
.5
1.
S^2

FIG. 2

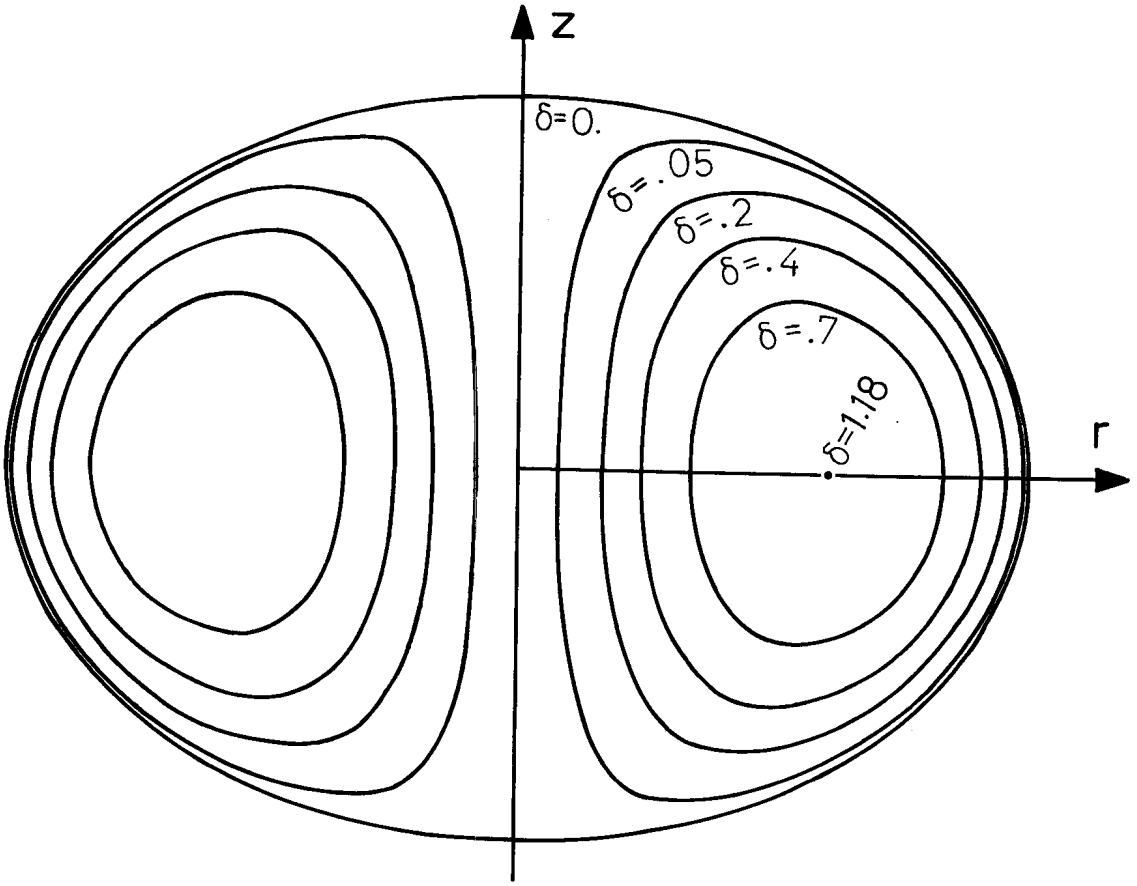

FIG. 3

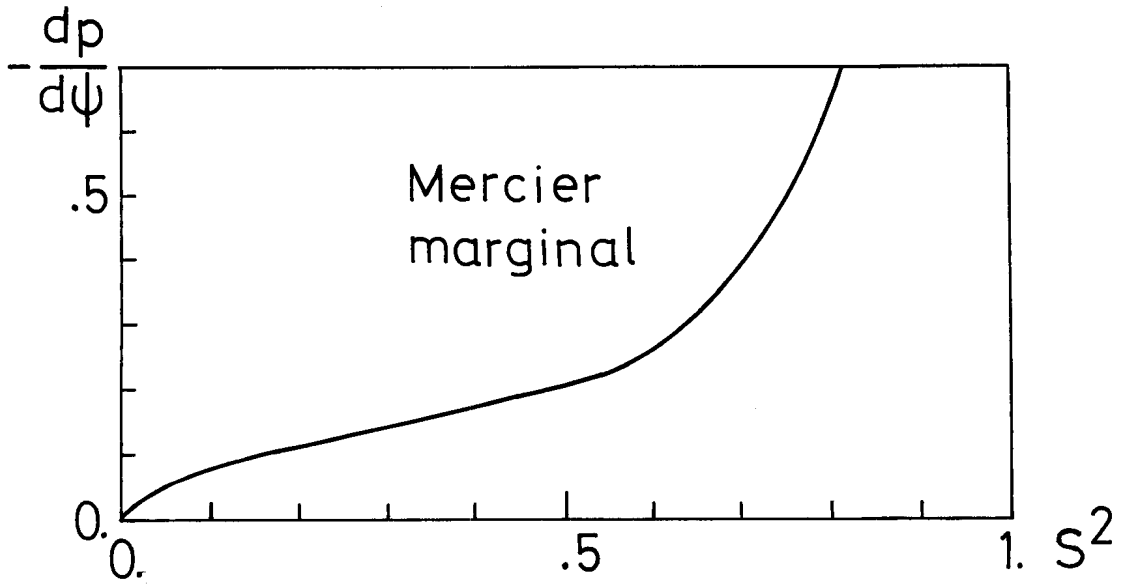

FIG. 4

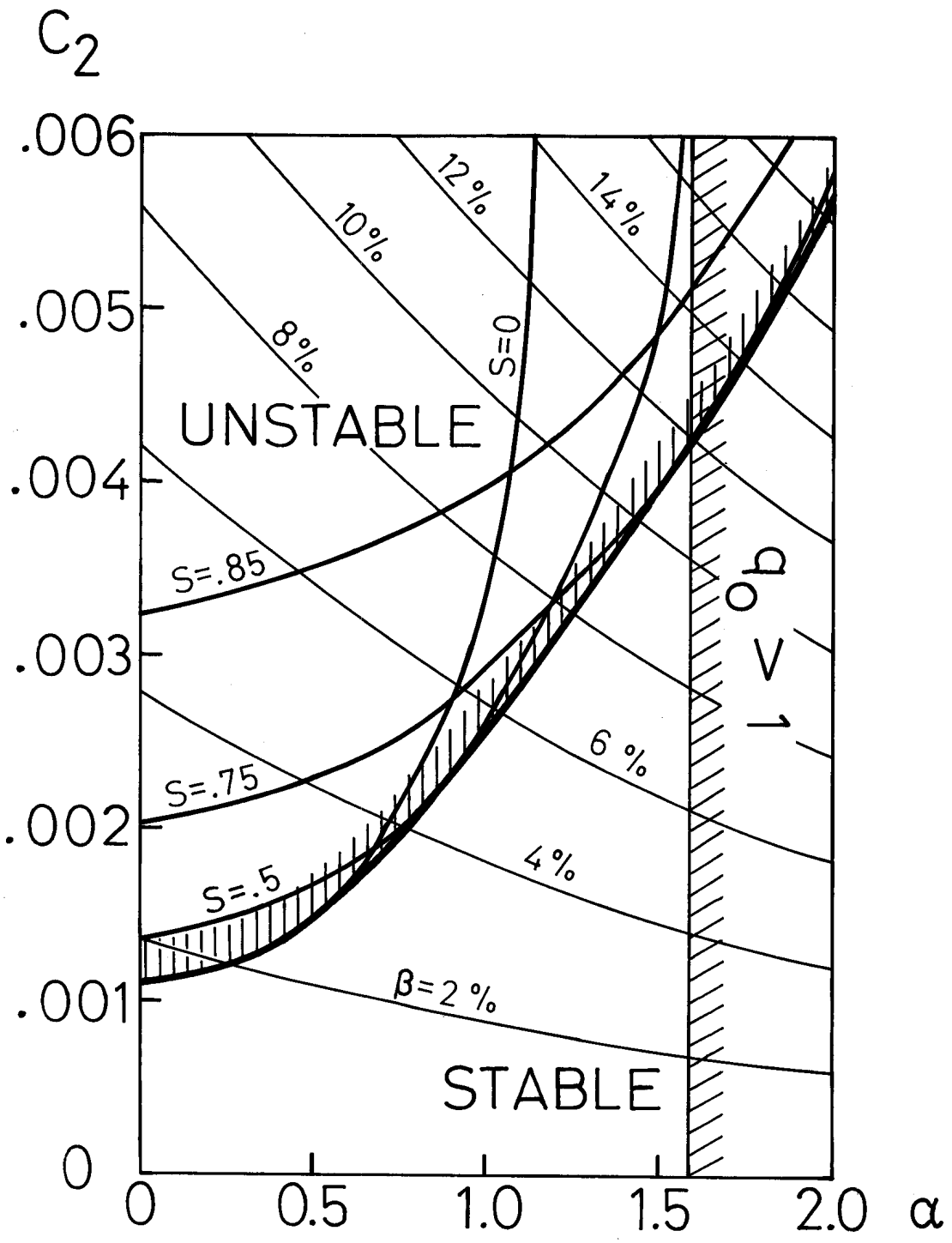
C2
.006
.005
.004
.003
.002
.001
0
0
0.5
1.0
1.5
2.0
α
12%
14%
10%
8%
S=0
UNSTABLE
S=.85
S=.75
S=.5
6%
4%
β=2%
STABLE
qo
V

FIG. 5

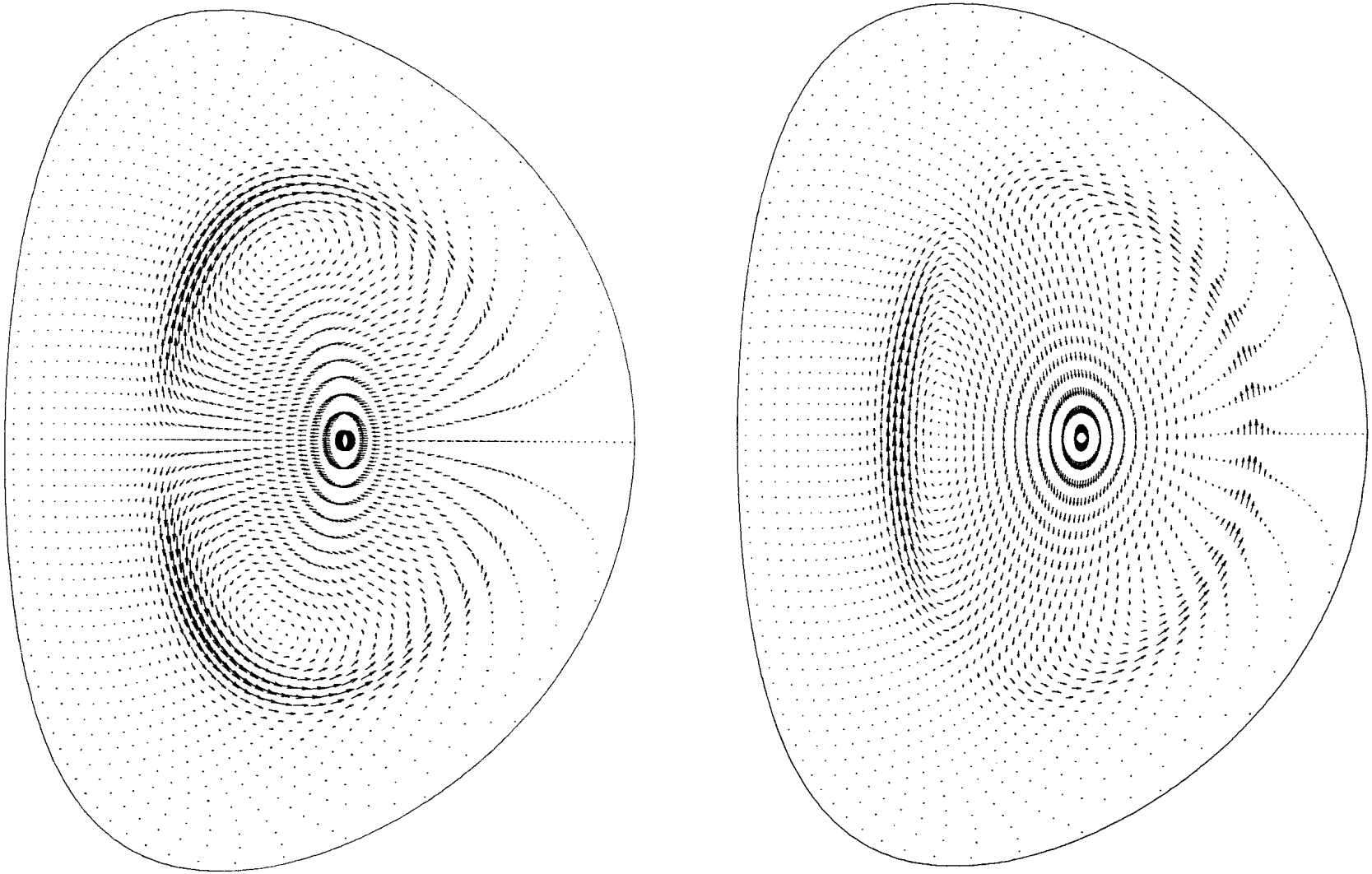

FIG. 6

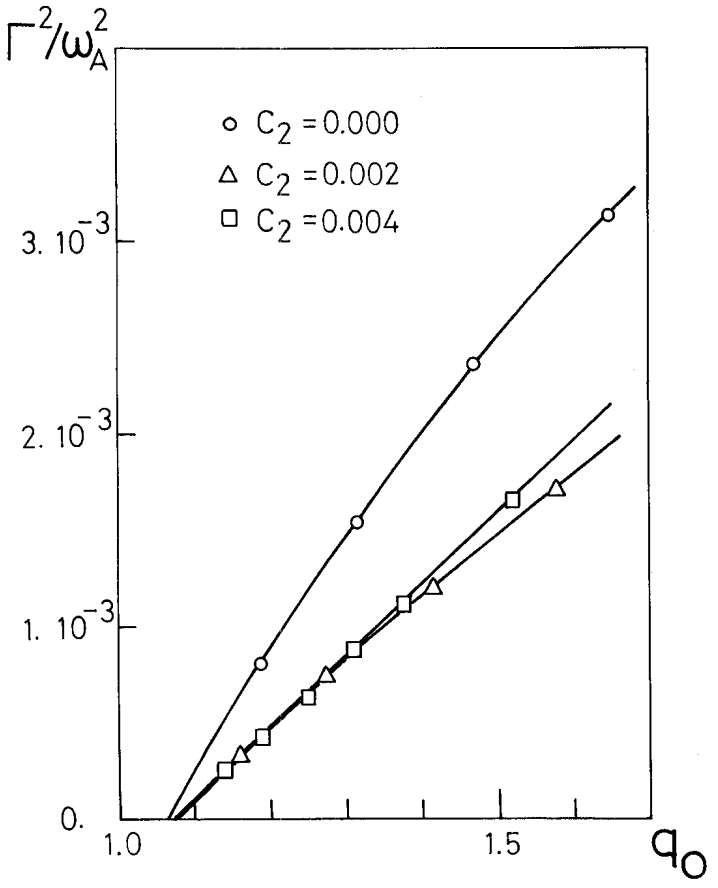
Γ^2/ω_A^2
$C_2 = 0.000$
$C_2 = 0.002$
$C_2 = 0.004$
$3.\ 10^{-3}$
$2.\ 10^{-3}$
$1.\ 10^{-3}$
0.
1.0
1.5
q_0

FIG. 7

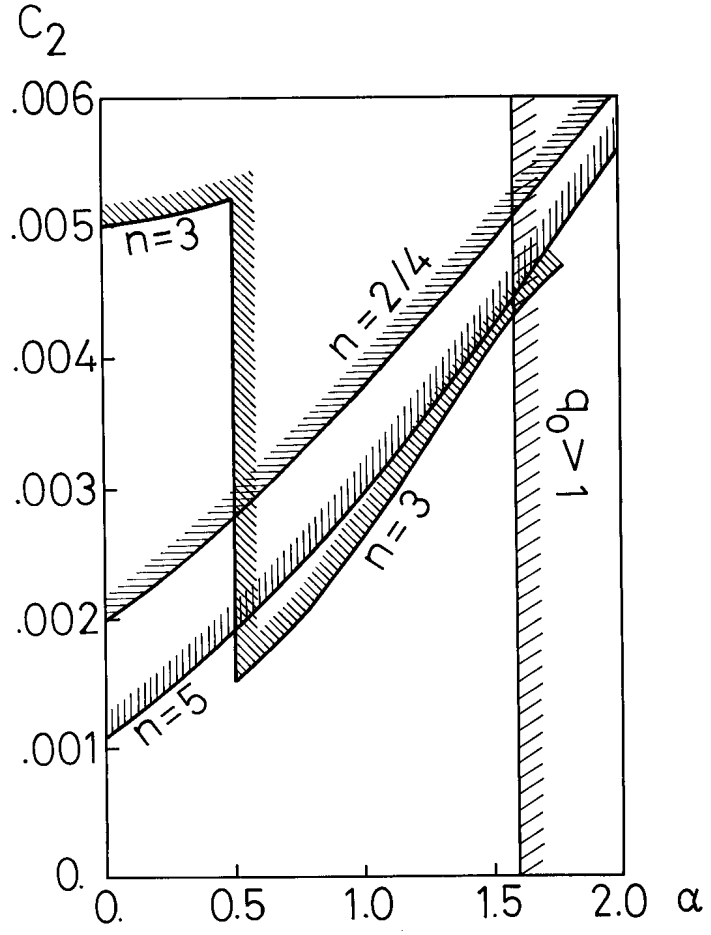
C_2
.006
.005
.004
.003
.002
.001
0.
n=3
n=2/4
n=3
n=5
$q_0 V 1$
0.
0.5
1.0
1.5
2.0
α

FIG. 8

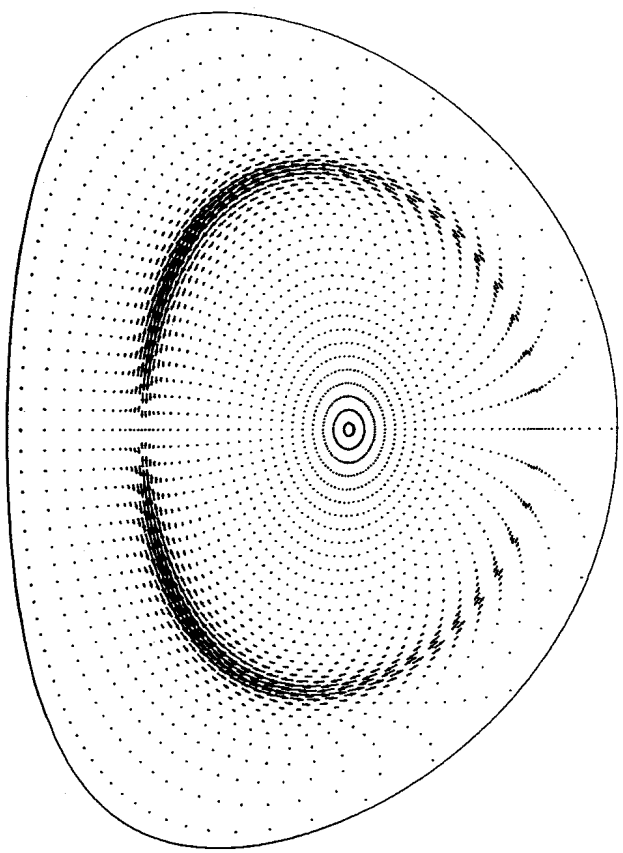

$C_2 = .006$

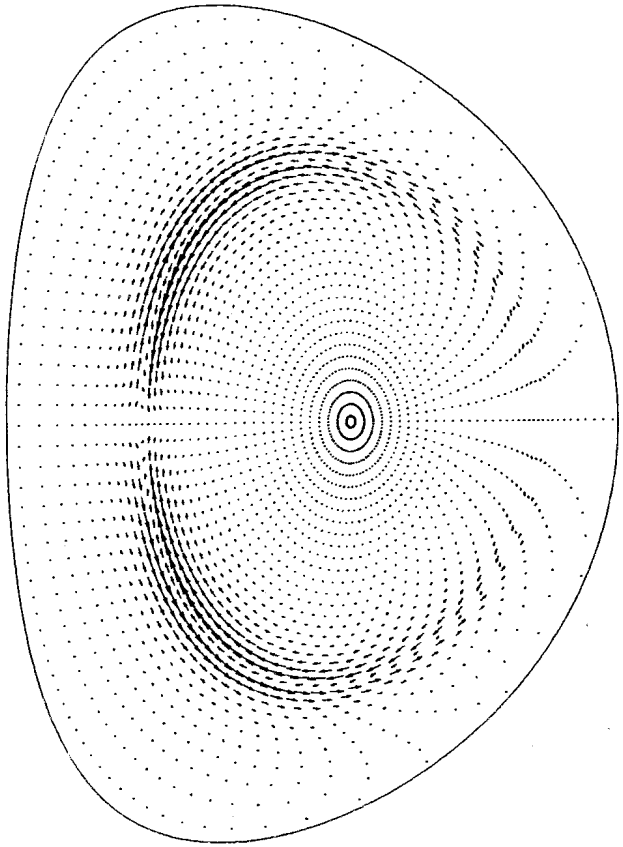

$C_2 = .008$

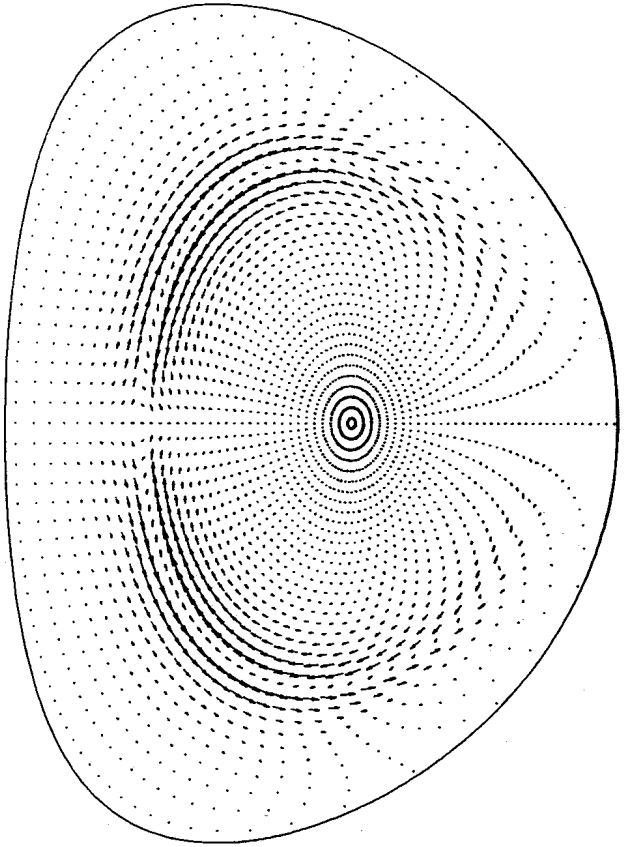

$C_2 = .010$

FIG. 9

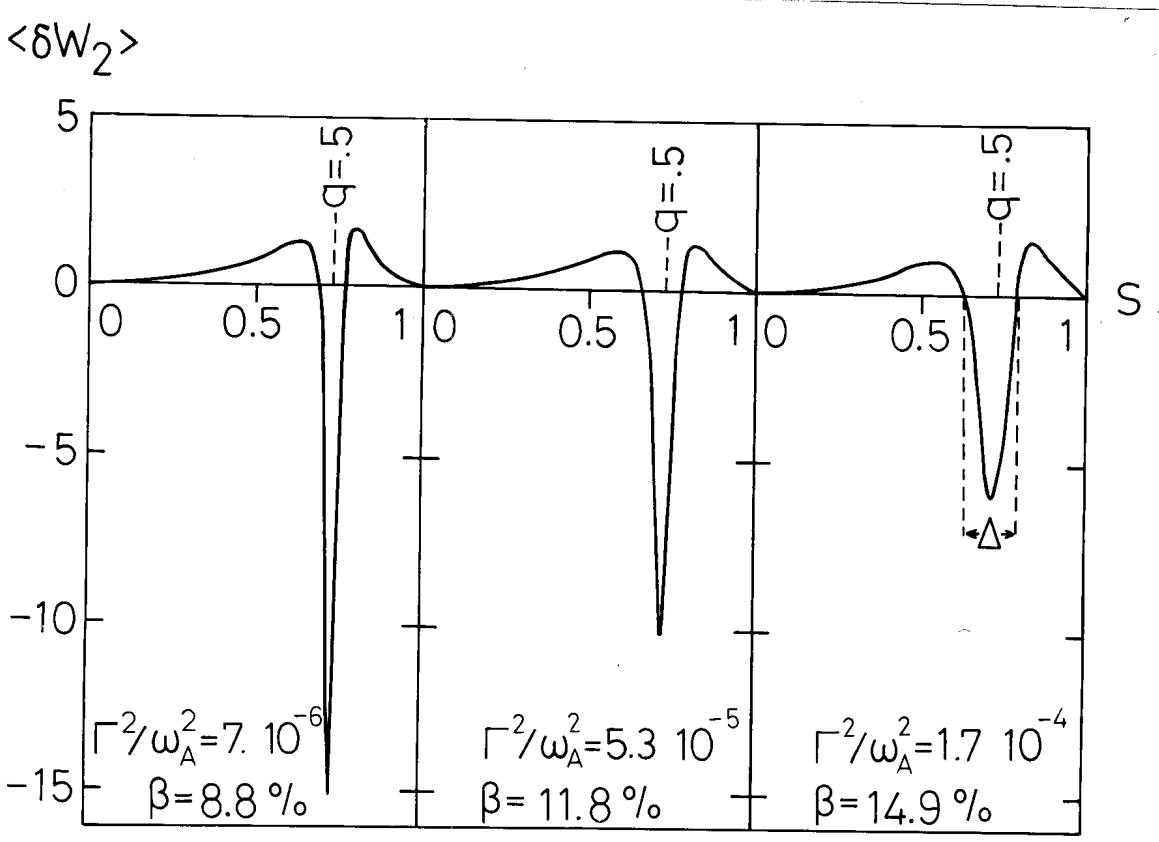
<δW2>
5
0
-5
-10
-15
0
0.5
1
q=5
S
Δ
Γ²/ω²A=7. 10⁻⁶
β=8.8 %
Γ²/ω²A=5.3 10⁻⁵
β= 11.8 %
Γ²/ω²A=1.7 10⁻⁴
β=14.9 %

FIG. 10

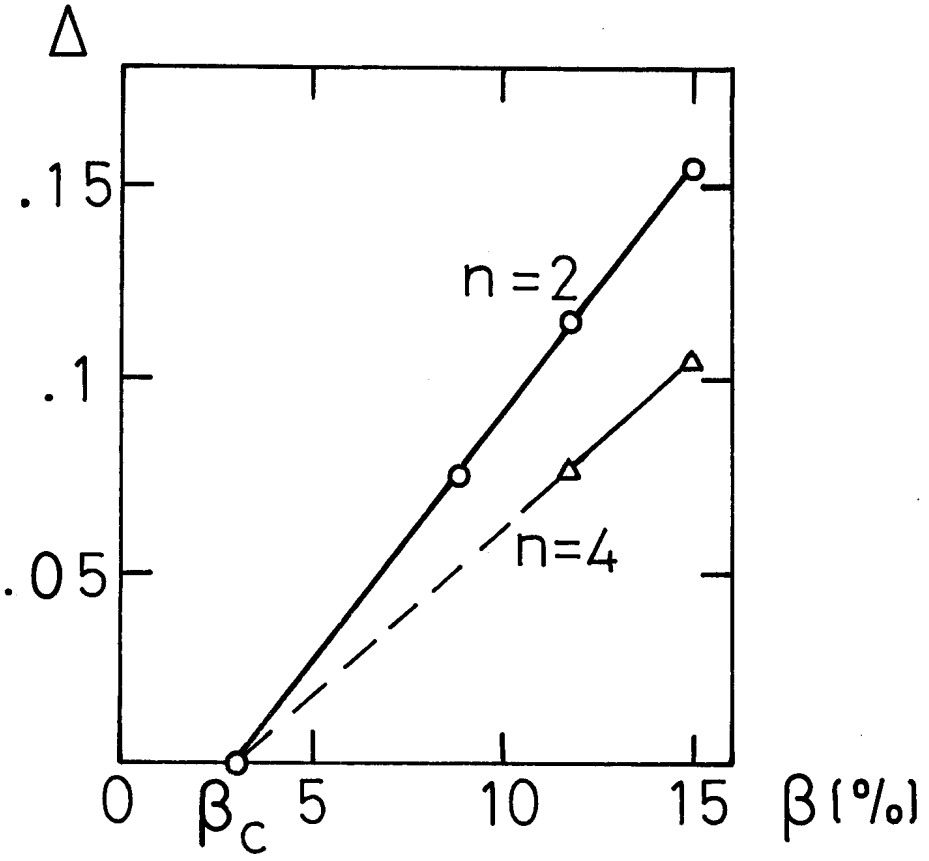
Δ
.15
.1
.05
n=2
n=4
0
βc
5
10
15
β(%)

FIG. 11

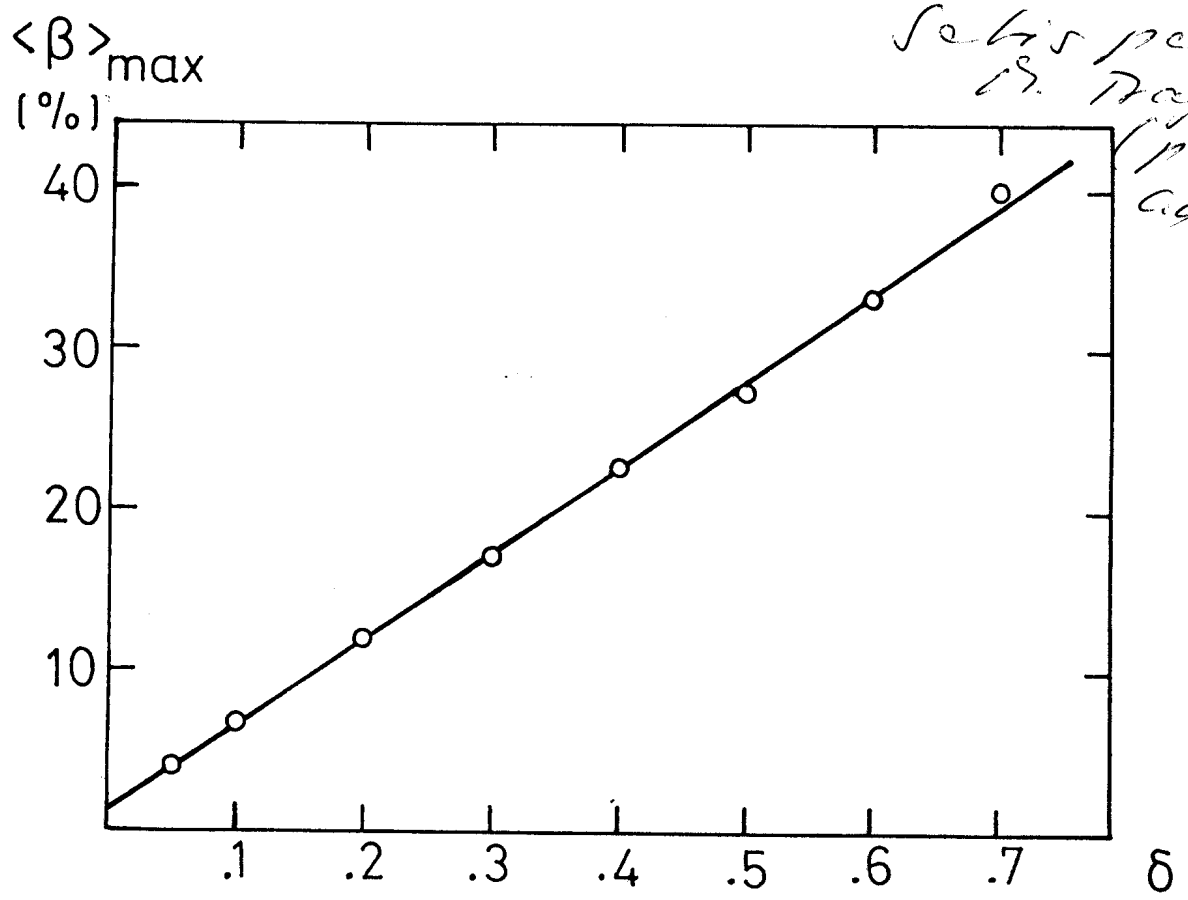
$\langle\beta\rangle_{max}$
(%)
40
30
20
10
.1
.2
.3
.4
.5
.6
.7
δ

FIG. 12

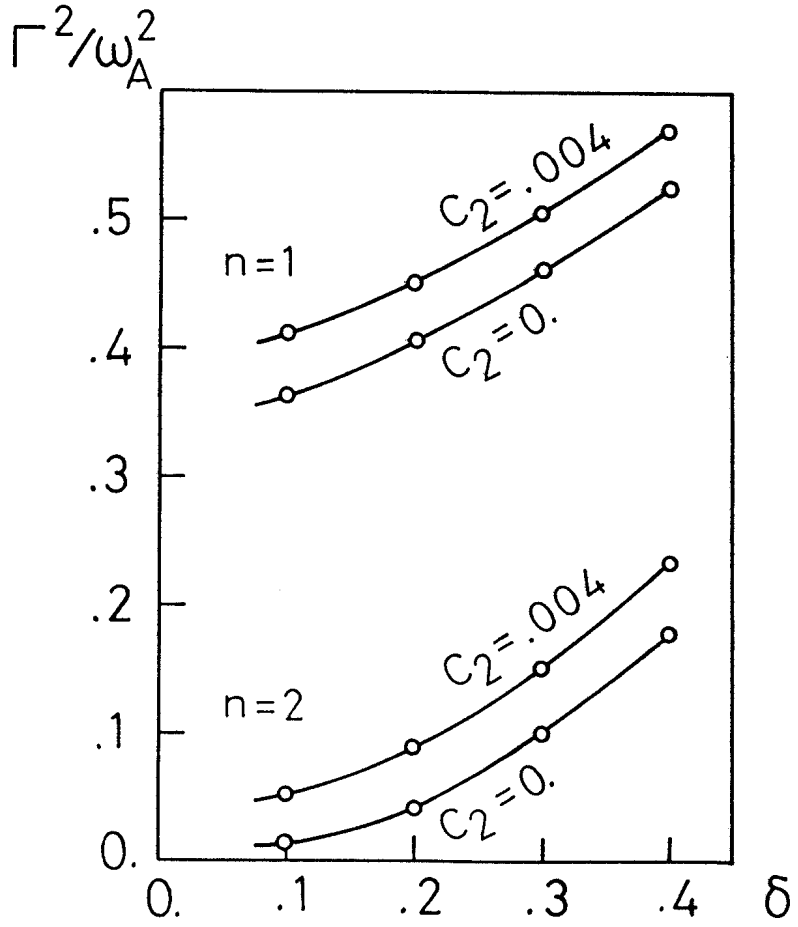
Γ^2/ω_A^2
.5
.4
.3
.2
.1
0.
n=1
C_2=.004
C_2=0.
n=2
C_2=.004
C_2=0.
0.
.1
.2
.3
.4
δ

FIG. 13

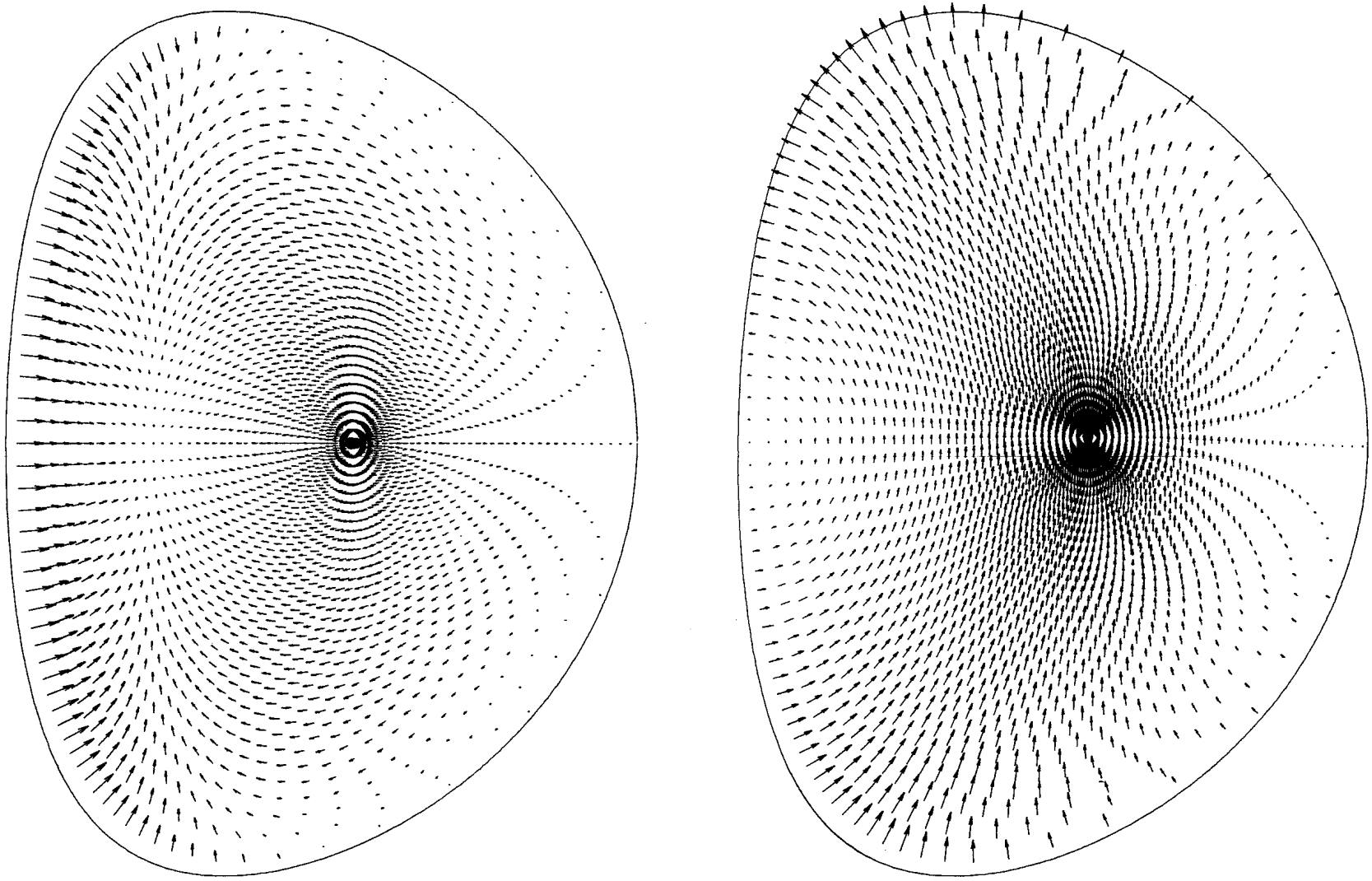

FIG. 14

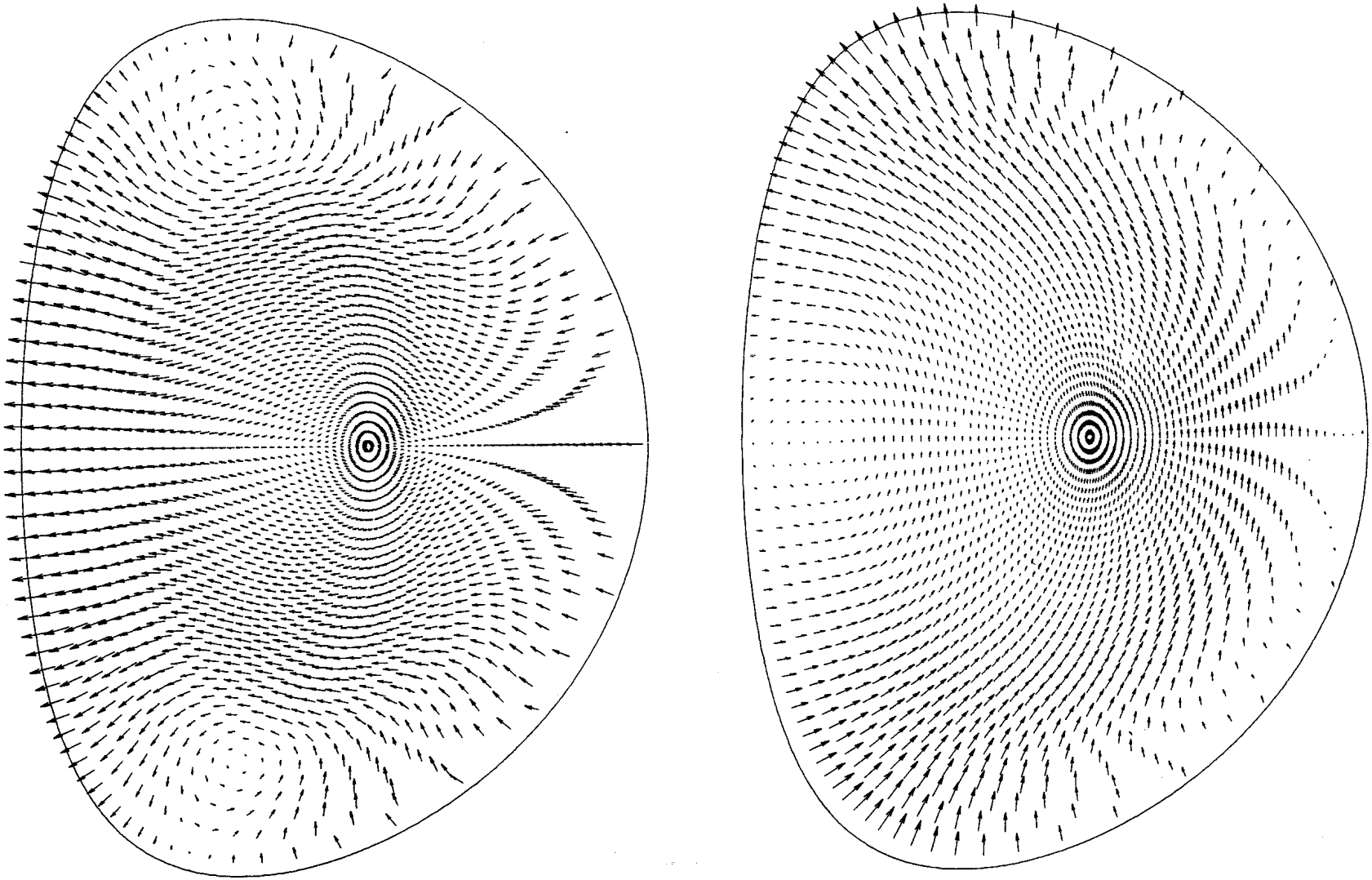

FIG. 15

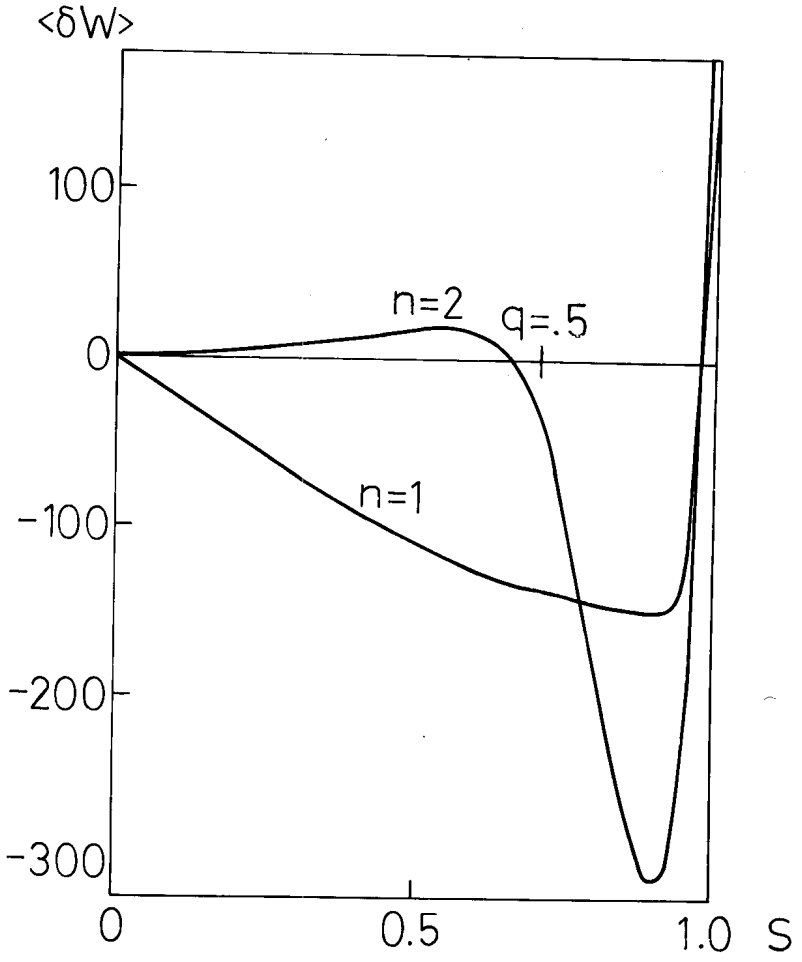
<δW>
100
0
-100
-200
-300
n=2
q=.5
n=1
0
0.5
1.0
S

FIG. 16

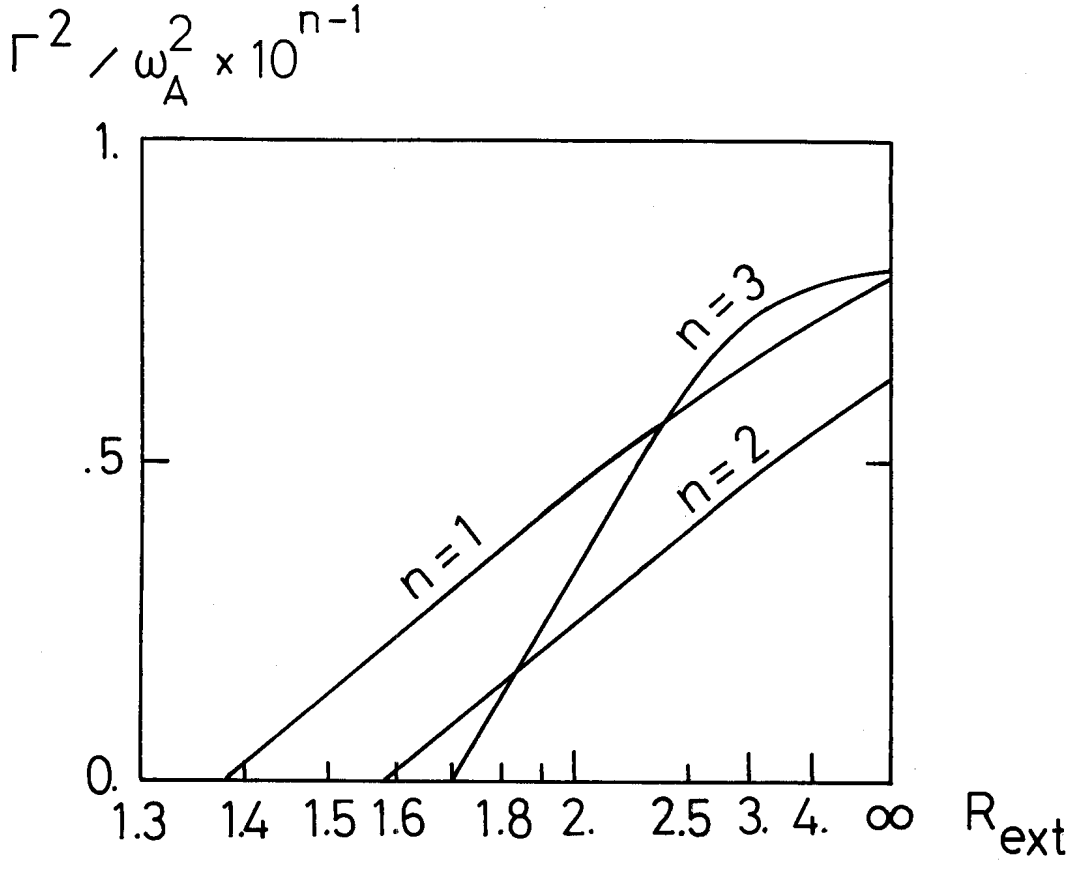
$\Gamma^2 / \omega_A^2 \times 10^{n-1}$
1.
.5
0.
n=3
n=2
n=1
1.3
1.4
1.5
1.6
1.8
2.
2.5
3.
4.
∞
R_{ext}

FIG. 17

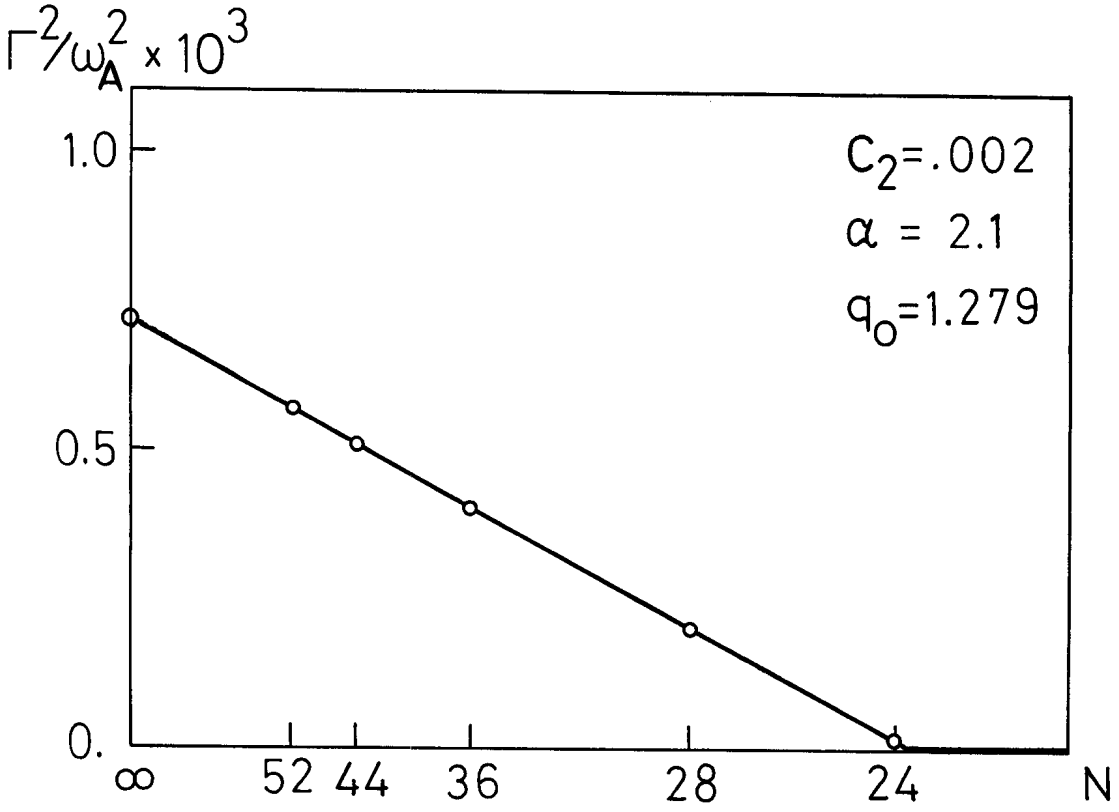
$\Gamma^2/\omega_A^2 \times 10^3$
1.0
0.5
0.
C_2=.002
α = 2.1
q_o=1.279
∞
52
44
36
28
24
N

FIG. 18